CCD Photometry, Light Curve Modeling and Period Study of V1073 Herculis, a Totally Eclipsing Overcontact Binary System

Kevin B. Alton
Desert Blooms Observatory, 70 Summit Avenue, Cedar Knolls, NJ 07927; kbalton@optonline.net

John C. Downing
La Ventana Observatory, 28881 Sunset Road, Valley Center, CA 92082; johndowning2014@outlook.com

Abstract   Precise time-series multi-color (BVI_c) light curve data were acquired from V1073 Her at Desert Blooms Observatory (DBO) in 2020 and La Ventana Observatory (LVO) in 2021. New times of minimum from data acquired at DBO and LVO along with other eclipse timings extracted from selected surveys and the literature were used to generate an updated linear ephemeris. Secular analyses (eclipse timing differences vs. epoch) revealed changes in the orbital period of V1073 Her over the past 22 years. Along with an apparent increase in the orbital period, the residuals after a parabolic fit of the data indicated that there was an underlying sinusoidal-like variability. This behavior suggests the putative existence of a third gravitationally bound object or cycles in magnetic activity, both of which are addressed herein. Simultaneous modeling of multicolor light curve data during each epoch was accomplished using the Wilson-Devinney code. Since a total eclipse is observed, a unique photometrically derived value for the mass ratio (q_{ptm}) could be determined which subsequently provided initial estimates for the physical and geometric elements of V1073 Her.

1. Introduction

Sparsely sampled monochromatic photometric data for V1073 Her (= NSVS 8092487) were first captured during the ROTSE-I survey between 1999 and 2000 (Akerlof *et al.* 2000; Wozniak *et al.* 2004). These data were retrieved from the Northern Sky Variable Survey (NSVS) archives. Blättler and Diethelm (2000) produced a complete unfiltered light curve (LC) for this eclipsing binary star (GSC 2625-1563) along with the first linear ephemeris. Gettel *et al.* (2006) included V1073 Her in their catalog of bright contact binary stars from the ROTSE-I survey. Other sources for photometric data from this variable system include the Catalina Sky Survey (Drake *et al.* 2014), the All-Sky Automated Survey for SuperNovae (ASAS-SN, Shappee *et al.* 2014; Jayasinghe *et al.* 2018), and the SuperWASP Survey (Butters *et al.* 2010). Samec *et al.* (2014) reported the first multi-color (BVR_c and I_c) LCs from V1073 Her which were modeled using the Wilson-Devinney code (Wilson and Devinney 1971; Wilson 1979, 1990). At that time secular analyses suggested the presence of a third gravitationally bound object which the authors proposed to be a brown dwarf. Our investigation of this overcontact binary (OCB) also includes Roche modeling of CCD-derived LCs as well as an in-depth secular analysis of the predicted vs. observed eclipse timing differences (ETD) over the past 22 years.

2. Observations and data reduction

Precise time-series images were acquired at Desert Blooms Observatory (DBO; 31.941 N, 110.257 W) using a QSI 683 wsg-8 CCD camera mounted at the Cassegrain focus of a 0.4-m Schmidt-Cassegrain telescope. A Taurus 400 (Software Bisque) equatorial fork mount facilitated continuous operation without the need to perform a meridian flip. The image (science, darks, and flats) acquisition software (THeSkyX Pro Edition 10.5.0;

Software Bisque 2019) controlled the main and integrated guide cameras.

This focal-reduced (f/7.2) instrument produces an image scale of 0.76 arcsec/pixel (bin=2×2) and a field-of-view (FOV) of 15.9×21.1 arcmin. Computer time was updated immediately prior to each session and exposure time for all images set to 75 s.

The equipment at La Ventana Observatory (LVO; 33.2418 N, 116.9781 W) included an iOptron CEM60 mount with an SBIG Aluma CCD694 camera installed at the Cassegrain focus of a 0.235-m Schmidt-Cassegrain telescope. TheSkyX Pro Edition 10.5.0 controlled the main (30-s exposures) and integrated guide cameras during image acquisition (science, darks, and flats). This focal-reduced (f/7) instrument produces an image scale of 1.14 arcsec/pixel (bin=2×2) and a field-of-view (FOV) of 26.1×20.9 arcmin.

Both CCD cameras were equipped with Astrodon B, V, R_c, and I_c filters manufactured to match the Johnson-Cousins Bessell specification. Dark subtraction, flat correction, and registration of all images collected at DBO and LVO were performed with AIP4WIN v2.4.0 (Berry and Burnell 2005).

Instrumental readings from V1073 Her were reduced to catalog-based magnitudes using APASS DR9 values (Henden *et al.* 2009, 2010, 2011; Smith *et al.* 2011) built into MPO Canopus v 10.7.1.3 (Minor Planet Observer 2010). LC data acquired in 2021 at LVO were only used to supplement ToM values for secular analyses.

3. Results and discussion

Light curves were generated using an ensemble of four comparison stars, each of which remained constant (<±0.01 mag) throughout every imaging session. The identity, J2000 coordinates, and color indices (B–V) for these stars are provided in Table 1. A CCD image annotated with the location of the target (T) and comparison stars (1–4) is shown in Figure 1.

Table 1. Astrometric coordinates (J2000), V-mags and color indices (B–V) for V1073 Her (Figure 1), and the corresponding comparison stars used in this photometric study.

Star Identification	R.A. (J2000)	Dec. (J2000)	V-mag[b]	(B–V)[b]
(T) V1073 Her	18 08 35.7571	+33 42 04.755	11.449	0.950
(1) GSC 2629-1797	18 08 55.4755	+33 45 45.118	11.341	0.863
(2) GSC 2629-1443	18 08 39.3063	+33 48 13.847	10.807	1.044
(3) GSC 2625-1672	18 08 22.8761	+33 38 25.825	11.343	0.813
(4) GSC 2625-1752	18 08 41.6918	+33 41 52.148	13.227	0.962

a. R.A. and Dec. from Gaia DR2 (Gaia Collab. et al. 2016, 2018).
b. V-mag and (B–V) for comparison stars derived from APASS DR9 database described by Henden et al. (2009, 2010, 2011) and Smith et al. (2011).

Table 2. Summary of image acquisition dates, number of data points and estimated uncertainty (± mag) in each bandpass (BVI$_c$) used for the determination of ToM values and/or Roche modeling.

n	Filter	(± mag)	Location	Dates
263	B	0.008	DBO	June 23–June 30, 2020
261	V	0.004	DBO	June 23–June 30, 2020
259	I$_c$	0.005	DBO	June 23–June 30, 2020
360	V	0.002	LVO	July 14–July 20, 2021

Table 3. Sample table of V1073 Her times-of-minimum (March 21, 1999–July 20, 2021), cycle number and residuals (ETD) between observed and predicted times derived from the updated linear ephemeris (Equation 1).

HJD–2400000	HJD Error	Cycle No.	ETD[a]	Reference
51258.8894	0.0008	–27718	0.0058	1
51277.8726	0.0004	–27653.5	0.0079	1
51746.3660	0.0120	–26061.5	0.0046	2
51746.5125	0.0008	–26061	0.0039	1
51768.4372	0.0003	–25986.5	0.0046	2

a. ETD = Eclipse Time Difference.
1. Blättler and Diethelm (2000); 2. Blättler et al. (2000). Full table available at: ftp://ftp.aavso.org/public/datasets/492-Alton-V1073Her.txt .
All references relevant to the full table that appears on the AAVSO ftp site are included in the References section of this article.

Table 4. Orbital period modulation (P$_3$) and putative third-body solution to the light-time effect (LiTE) observed from changes in V1073 Her eclipse timings.

Parameter	Units	LiTEa
HJD$_0$–2400000		2451258.8899 ± 0.0007
P$_3$	(y)	13.678 ± 0.259
A (semi-ampl.)	(d)	0.00309 ± 0.00042
ω	(°)	0
e$_3$		0 ± 0.1
a'$_{12}$ sin i'	(a.u.)	0.5349 ± 0.0733
f(M$_3$) (mass func.)	(M$_\odot$)	0.00082 ± 0.00004
M$_3$ (i = 90°)	(M$_\odot$)	0.126 ± 0.002
M$_3$ (i = 60°)	(M$_\odot$)	0.146 ± 0.003
M$_3$ (i = 30°)	(M$_\odot$)	0.266 ± 0.005
Q (quad. coeff.)	(10^{-10})	0.3511 ± 0.0001
Sum of squared residuals		0.002542

a. Zasche et al. (2009)—simplex optimization with third body circular orbit.

Table 5. Estimation of effective temperature (T$_{eff1}$) of the primary star in V1073 Her.

Parameter	V1073 Her
DBO (B–V)$_0$	0.927 ± 0.028
Median combined (B–V)$_0$[a]	0.916 ± 0.023
Galactic reddening E(B–V)[b]	0.0337 ± 0.0001
Survey T$_{eff1}$[c] (K)	4990 ± 47
Gaia T$_{eff1}$[d] (K)	5506$^{+583}_{-264}$
Houdashelt T$_{eff1}$[e] (K)	5002 ± 360
Median T$_{eff1}$ (K)	5166 ± 201
Spectral Class[f]	K1V-K2V

a. Surveys and DBO intrinsic (B–V)$_0$ determined using reddening values (E(B–V)).
b. Model A (http://www.galextin.org/).
c. T$_{eff1}$ interpolated from median combined (B–V)$_0$ using Table 4 in Pecaut and Mamajek (2013).
d. Values from Gaia DR2 (Gaia Collab. et al. 2016, 2018) (http://vizier.u-strasbg.fr/viz-bin/VizieR?-source=I/345/gaia2).
e. Values calculated with Houdashelt et al. (2000) empirical relationship.
f. Spectral class estimated from Pecaut and Mamajek (2013).

Table 6. Light curve parameters evaluated by Roche modeling and the geometric elements derived for V1073 Her (2019) assuming it is a W-type W UMa variable.

Parameter	DBO No spot	DBO Spotted	Samec et al. (2014) Spotted
T$_{eff1}$ (K)[b]	5166	5166	5150
T$_{eff2}$ (K)	5317 (3)	5296 (3)	5176 (1)
q (m$_2$/m$_1$)	0.379 (1)	0.386 (3)	0.404 (4)
A[b]	0.50	0.50	0.50
g[b]	0.32	0.32	0.32
Ω$_1$ = Ω$_2$	2.612 (3)	2.627 (3)	2.640 (4)
i°	84.1 (3)	83.5 (2)	82.3 (1)
A$_P$ = T$_S$ / T$_{star}$[c]	—	0.90 (2)	—
Θ$_P$ (spot co-latitude)[c]	—	104 (5)	—
Φ$_P$ (spot longitude)[c]	—	199 (5)	—
r$_P$ (angular radius)[c]	—	9.0 (2)	—
A$_S$ = T$_S$/T$_{star}$[c]	—	—	0.861 (5)
Θ$_S$ (spot co-latitude)[c]	—	—	93 (2)
Φ$_S$ (spot longitude)[c]	—	—	244 (1)
r$_S$ (angular radius)[c]	—	—	21.8 (3)
L$_1$/(L$_1$+L$_2$)B[d]	0.6649 (2)	0.6674 (2)	0.652 (1)
L$_1$/(L$_1$+L$_2$)V	0.6749 (2)	0.6760 (1)	0.658 (1)
L$_1$/(L$_1$+L$_2$)I$_c$	0.6845 (1)	0.6843 (2)	0.663 (1)
L$_1$/(L$_1$+L$_2$)R$_c$	—	—	0.660 (1)
r$_1$ (pole)	0.4415 (4)	0.4398 (4)	0.440 (1)
r$_1$ (side)	0.4728 (5)	0.4708 (4)	0.472 (2)
r$_1$ (back)	0.5009 (6)	0.4989 (5)	0.502 (2)
r$_2$ (pole)	0.2831 (12)	0.2842 (11)	0.292 (1)
r$_2$ (side)	0.2957 (15)	0.2969 (13)	0.306 (2)
r$_2$ (back)	0.3317 (26)	0.3327 (23)	0.345 (4)
Fill-out factor (%)	10	9.5	18
RMS (B)[e]	0.00848	0.00871	—
RMS (V)	0.00789	0.00749	—
RMS (I$_c$)	0.00658	0.00603	—

a. All DBO uncertainty estimates for T$_{eff2}$, q, Ω$_{1,2}$, i, r$_{1,2}$, and L$_1$ from WDwint56a (Nelson 2009).
b. Fixed with no error during DC.
c. Spot parameters in degrees (Θ$_{P,S}$, Φ$_{P,S}$, and r$_{P,S}$) or A$_{P,S}$ in fractional degrees (K).
d. L$_1$ and L$_2$ refer to scaled luminosities of the primary and secondary stars, respectively.
e. Monochromatic residual mean square error from observed values.

Table 7. Fundamental stellar parameters for V1073 Her using the photometric mass ratio ($q_{ptm} = m_2/m_1$) from the spotted Roche model fits of LC data (2020) and the estimated primary star mass based on empirically derived M-PRs for overcontact binary systems.

Parameter	Primary	Secondary
Mass ($M_\odot$)	1.026 ± 0.017	0.396 ± 0.006
Radius ($R_\odot$)	0.970 ± 0.004	0.629 ± 0.003
a ($R_\odot$)	2.094 ± 0.009	2.094 ± 0.009
Luminosity ($L_\odot$)	0.603 ± 0.094	0.280 ± 0.002
Mbol	5.299 ± 0.009	6.132 ± 0.009
Log (g)	4.476 ± 0.008	4.439 ± 0.008
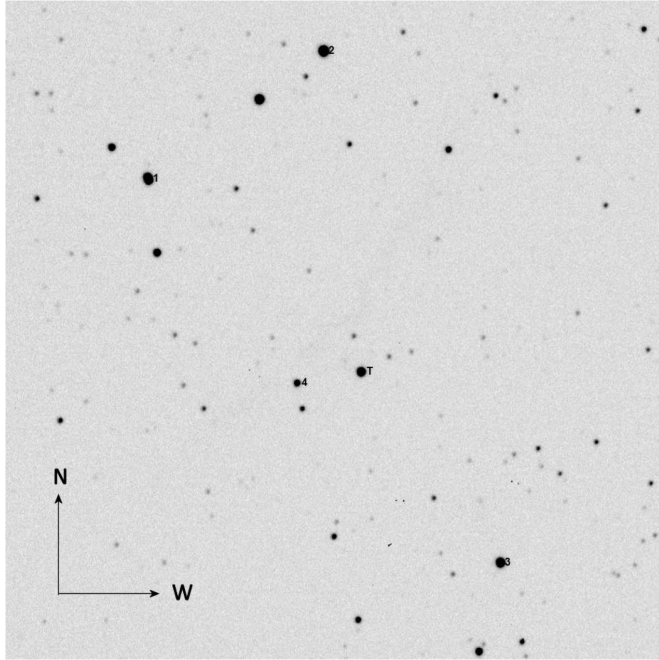
Figure 1. CCD image (V mag) of V1073 Her (T) acquired at DBO showing the location of comparison stars (1–4) used to generate APASS DR9-derived magnitude estimates.
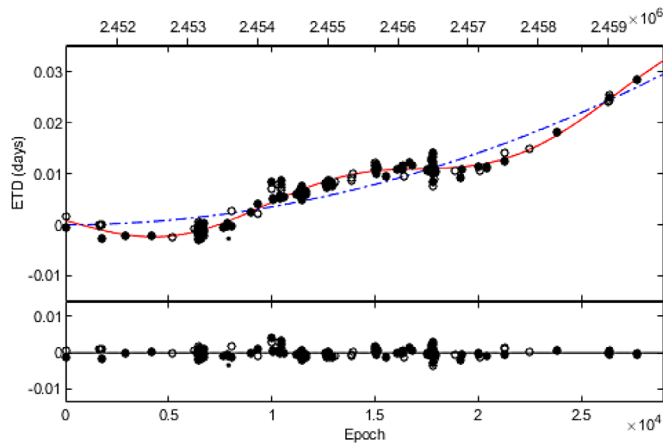
Figure 2. LiTE fit (Table 4) using eclipse timing differences (ETD) determined for V1073 Her between 1999 and 2021. The solid red line in the top panel describes the fit for a circular (e = 0) orbit ($P_3 = 13.678 \pm 0.259$ y) of a putative third body while the dashed blue line defines the quadratic fit from the eclipse timing residuals. Solid circles (●) represent times at Min I whereas open circles (○) indicate times at Min II. The bottom panel illustrates the total residuals remaining after LiTE analysis after subtracting out the quadratic component.
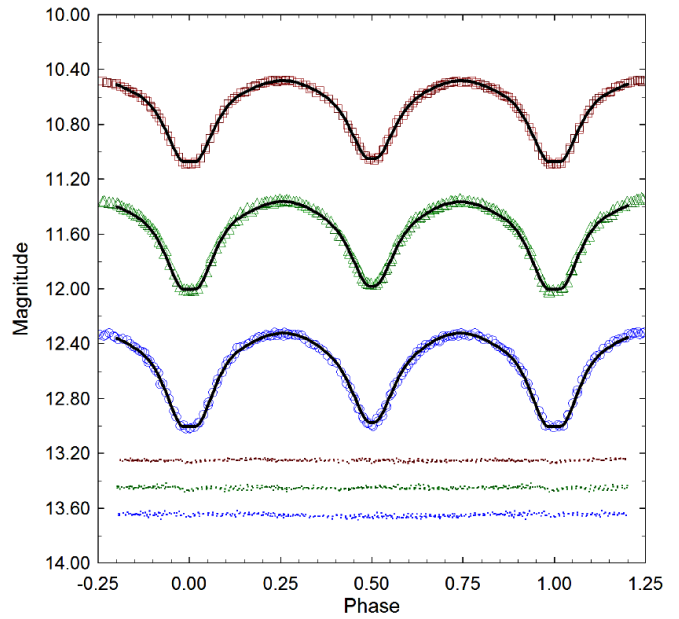

Figure 3. Period folded (0.2942818 ± 0.0000001 d) CCD-derived LCs for V1073 Her produced from photometric data collected at DBO between June 23, 2020 and June 30, 2020 The top (I_c), middle (V), and bottom curve (B) were transformed to magnitudes based on APASS DR9-derived catalog values from comparison stars. In this case, the Roche model assumed a W-subtype overcontact binary with single spot on the most massive star; residuals from the model fits are offset at the bottom of the plot to keep the values on scale.
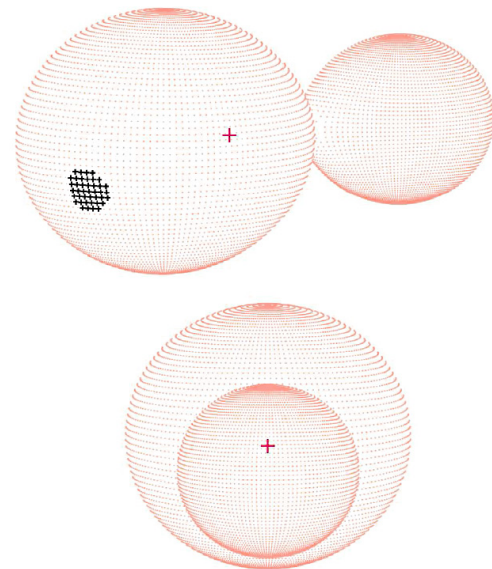

Figure 4. Three-dimensional spatial model of V1073 Her during 2020 illustrating (top) the location of a cool (black) spot on the primary star and (bottom) the secondary star transit across the primary star face at Min II ($\Phi = 0.5$).

Only data acquired above 30° altitude (airmass < 2.0) were included; differential atmospheric extinction was ignored considering the close proximity of all program stars. All photometric data can be retrieved from the AAVSO International Database via the International Variable Star Index (Watson *et al.* 2014).

3.1. Photometry and ephemerides

Times of minimum (ToM) and associated errors were calculated using the method of Kwee and van Woerden (1956) as implemented in Peranso v2.5 (Paunzen and Vanmunster 2016). Curve fitting all eclipse timing differences (ETD) was accomplished using scaled Levenberg-Marquardt algorithms (QTiPlot 0.9.9-rc9; IONDEV SRL 2021). Photometric uncertainty was calculated according to the so-called "CCD Equation" (Mortara and Fowler 1981; Howell 2006). The acquisition dates, number of data points, and uncertainty for each bandpass used for the determination of ToM values and/ or Roche modeling are summarized in Table 2.

Six new ToM measurements were extracted from photometric data acquired at DBO and LVO. The SuperWASP survey (Butters *et al.* 2010) provided a wealth of photometric data taken (30-s exposures) at modest cadence that repeats every 9 to 12 min. In some cases (n = 68) these SuperWASP data were amenable to further analysis using the method of Kwee and van Woerden (1956) to estimate ToM values. These, along with 156 other eclipse timings (Table 3) from the literature, were used to calculate a new linear ephemeris based on data produced between 1999 and 2021:

$$\text{Min. I (HJD)} = 2459415.7874\,(4) + 0.2942818\,(1)\,E. \quad (1)$$

For the purpose of illustration the first five entries in Table 3 are provided herein; all values will be web-archived and made available through the AAVSO ftp site at:

ftp:ftp.aavso.org/public/datasets/492-Alton-V1073Her.txt .

A sinusoidal-like variation was found embedded within the residuals remaining after the initial linear fit (Figure 2). Cyclic changes of eclipse timings can result from the gravitational influence of unseen companion(s), the so-called light-time effect (LiTE). It is not unreasonable to propose that V1073 Her is a ternary system since a significant number (> 50%) of contact binaries observed from the Northern Hemisphere exist as multiple systems (Pribulla and Ruciński 2006). To address this possibility LiTE analyses were performed using the simplex code for MATLAB® reported by Zasche *et al.* (2009).

A quadratic relationship between ETD and epoch takes the general form:

$$\text{ETD}_{\text{fitted}} = c + b \cdot E + Q \cdot E^2 + \tau. \quad (2)$$

When the orbital period change is monotonic, the last term ($\tau = 0$) can be ignored. However, in this case τ from Equation 2 is expanded as follows:

$$\tau = \frac{a_{12}\sin i_3}{c}\left[(1-e^2)\frac{\sin(\nu+\omega)}{1+e\cdot\cos\nu}+\sin\omega\right] \quad (3)$$

Accordingly, the associated parameters in the LiTE equation (Irwin 1959) were derived, which include parameter values for P_3 (orbital period of star 3 and the 1–2 pair about the barycenter), orbital eccentricity e, argument of periapsis ω, true anomaly ν, time of periastron passage T_0, and amplitude $A = a_{12}\sin i_3$. In this case a_{12} is the semi-major axis of the 1–2 pair's orbit about the three-star system center of mass, and i_3 is the orbital inclination of the putative third body in a three-star system.

A single best fit to all the ETD residuals was produced with the Zasche *et al.* (2009) LiTE code using simplex optimization (Table 4). These results are consistent with a putative third body in a circular orbit ($P_3 = 13.678$ y) at a distance no farther than 5.57 ± 0.16 A.U. from the barycenter. The minimum mass of a coplanar ($i_3 = 90°$) orbiting third body was calculated to be $\sim 0.126 \pm 0.002\,M_\odot$, based on the derived mass function ($f(M_3) = 0.00082 \pm 0.00004$). A brown dwarf is expected to have a mass less than $0.075\,M_\odot$, therefore our LiTE model results do not support earlier speculation by Samec *et al.* 2014 about an orbiting brown dwarf. The corresponding added luminosity (L_3) of a third main sequence star ($M < 0.126\,M_\odot$) was estimated to be $\approx 0.22\%$ according to:

$$L_3\,(\%) \approx \frac{100 \cdot 0.23\,M_{\min}^{2.3}}{L_1 + L_2 + 0.23\,M_{\min}^{2.3}}, \quad (4)$$

where $M_{\min}$ is the estimated minimum mass ($i_3 = 90°$) in solar units. This very small percent contribution of light would not be expected nor did it require adjustment by the WD 2003 code third light parameter ($l_3 = 0$) in order to accurately simulate the LC model fits around minimum light (section 3.4).

Modulated changes in the orbital period can also result from magnetic activity cycles attributed to Applegate (1992) or apsidal motion of a binary pair. Since contact binary systems are tidally locked with circular orbits, apsidal motion can be immediately eliminated from consideration. Short-period binaries are magnetically very active due to the formation of photospheric (starspots), chromospheric (plages), and other high energy disturbances (Berdyugina 2005). The corresponding hydromagnetic dynamo can produce changes in the gravitational quadrupole moment of the active star via redistribution of the internal angular momentum with corresponding changes in the magnetic torque within the stellar convective zone. When the gravitational quadrupole moment of the active component increases, its companion experiences a stronger gravitational force which then moves closer to the system barycenter. The orbital period will decrease according to this scenario. By contrast, when the gravitational quadrupole moment of the active star weakens, the orbital period increases. A detailed examination of the energetics ($\Delta E / E_{\text{sec}}$) required to produce the "Applegate effect" was performed according to Völschow *et al.* (2016) and the accompanying "Eclipse Time Variation Calculator" webmodule[1]. $\Delta E / E_{\text{sec}}$ is defined as the energy required to drive the Applegate mechanism divided by the available energy produced in the magnetically active star. This value determines whether the Applegate mechanism is energetically feasible. Solutions are provided from the two-zone model and the constant density model by Völschow *et al.* (2016), along with a solution based on the thin-shell model

[1] http://theory-starformation-group.cl/applegate/index.php

by Tian *et al.* (2009). Tian *et al.* (2009) derived a relationship between the energetics necessary to drive the Applegate mechanism and the observed variability in eclipse timings:

$$\frac{\Delta E}{E_{sec}} = 0.233 \cdot \left(\frac{M_{sec}}{M_\odot}\right)^3 \cdot \left(\frac{R_{sec}}{R_\odot}\right)^{-10} \cdot \left(\frac{T_{sec}}{6000\,K}\right)^{-4} \cdot$$

$$\left(\frac{a_{bin}}{R_\odot}\right)^4 \cdot \left(\frac{\Delta P}{s}\right)^2 \cdot \left(\frac{P_{mod}}{yr}\right)^{-1}. \quad (5)$$

The measureables in this case include the secondary mass (M_{sec}), radius (R_{sec}), temperature (T_{sec}), semi-major axis of the binary pair (a_{bin}), the modulation period of the binary pair (P_{mod}), and ΔP where:

$$\frac{\Delta P}{P_{bin}} = 2\pi \left(\frac{O-C}{P_{mod}}\right). \quad (6)$$

Since the $\Delta E / E_{sec}$ value (0.62) is less than one, this would energetically favor orbital period modulations that arise from the Applegate mechanism.

The two-zone model provides two solutions, one requiring more energy and one requiring less energy. Therein the finite shell two-zone model accounts for all essential physics involved with the Applegate effect from main-sequence low mass companions ($0.1–0.6\,M_\odot$). Accordingly, the latter energy solution is:

$$\frac{\Delta E^-}{E_{sec}} = k_1 \cdot \frac{M_{sec}\,R_{sec}^2}{P_{bin}^2\,P_{mod}\,L_{sec}} \cdot$$

$$\left(1 \pm \sqrt{(1-k_2 G)\frac{a_{bin}^2\,M_{sec}\,P_{bin}^2}{R_{sec}^5}\quad\frac{\Delta P}{P_{bin}}}\,\right)^2, \quad (7)$$

wherein k_1 is assigned a value of 0.133 and k_2 is 3.42. Since the calculated value for $\Delta E / E_{sec}$ is less than unity (0.034), this model also indicates that V1073 Her is a potential candidate for orbital period modulation by magnetic cycles.

The apparent sinusoidal-like behavior is supported by data collected over the past 22 y, which is less than two cycles of orbital period variation. Therefore, some caution should be exercised in that these findings are considered preliminary and not a definitive solution. Furthermore at this time it is not possible to firmly establish whether the gravitational effect of a third body or variations in the quadrapole moment is responsible for cyclic changes in the orbital period of V1073 Her. Unfortunately without other supporting evidence such as might be derived from space-based spectro-interferometry and/or direct imaging, secular analysis still leaves us with two equally plausible but distinctly different phenomenological origins for cyclic modulation of the dominant orbital period.

3.2. Effective temperature estimation

The effective temperature (T_{eff1}) of the more massive, and therefore most luminous component (defined as the primary star

herein) was derived from a composite of photometric (USNO-B1, UCAC4, 2MASS, and APASS) determinations that were as necessary transformed to (B–V)[2, 3]. Interstellar extinction (A_V) and reddening ($E(B–V)=A_V/3.1$) were estimated for targets within the Milky Way Galaxy according to Amôres and Lépine (2005). These models[4] require the Galactic coordinates (l, b) and the distance in kpc estimated from Gaia DR2 derived parallax (Bailer-Jones 2015). After subtracting out reddening to arrive at a value for intrinsic color, $(B–V)_0$, T_{eff1} estimates were interpolated for each system using the values reported for main sequence dwarf stars by Pecaut and Mamajek (2013). Additional sources used to establish a median value for each T_{eff1} included the Gaia DR2 release of stellar parameters (Andrae *et al.* 2018), and an empirical relationship (Houdashelt *et al.* 2000) based on intrinsic color where $0.32 \le (B–V)_0 \le 1.35$. The median result ($T_{eff1}=5166\pm201$ K), summarized in Table 5, was adopted for Roche modeling of LCs from V1073 Her.

3.3. Roche modeling approach

Roche modeling of LC data from 2020 was initially performed with PHOEBE 0.31a (Prša and Zwitter 2005) and then refined using WDwint56a (Nelson 2009). Both programs feature a MS Windows-compatible GUI interface to the Wilson-Devinney WD2003 code (Wilson and Devinney 1971; Wilson 1979, 1990). WDwint56a incorporates Kurucz's atmosphere models (Kurucz 2002) that are integrated over BVI_c passbands. The final selected model was Mode 3 for an overcontact binary; other modes (detached and semi-detached) never approached the best fit value achieved with Mode 3. Modeling parameters were adjusted as follows. The internal energy transfer to the stellar surface is driven by convective (7500 K) rather than radiative processes. As a result, the value for bolometric albedo ($A_{1,2}=0.5$) was assigned according to Ruciński (1969) while the gravity darkening coefficient ($g_{1,2}=0.32$) was adopted from Lucy (1967). Logarithmic limb darkening coefficients (x_1, x_2, y_1, y_2) were interpolated (van Hamme 1993) following any change in the effective temperature (T_{eff2}) of the secondary star during model fit optimization using differential corrections (DC). All but the temperature of the more massive star (T_{eff1}), $A_{1,2}$ and $g_{1,2}$ were allowed to vary during DC iterations. In general, the best fits for T_{eff2}, i, q and Roche potentials ($\Omega_1=\Omega_2$) were collectively refined (method of multiple subsets) by DC using the multicolor LC data until a simultaneous solution was found. Surface inhomogeneity often attributed to star spots was simulated by the addition of a cool spot on the primary star to obtain the best fit LC models around Min I. V1073 Her did not require third light correction ($l_3=0$) to improve Roche model fits.

3.4. Roche modeling results

Without radial velocity (RV) data it is generally not possible to unambiguously determine the mass ratio, subtype (A or W), or total mass of an eclipsing binary system. Nonetheless, since a total eclipse is observed, a unique mass ratio value could be found (Terrell and Wilson 2005). Standard errors reported in Table 6 are computed from the DC covariance matrix and only reflect the model fit to the observations which assume exact values for any fixed parameter. These errors are generally

regarded as unrealistically small considering the estimated uncertainties associated with the mean adopted T_{eff1} values along with basic assumptions about $A_{1,2}$, $g_{1,2}$, and the influence of spots added to the Roche model. Normally, the value for T_{eff1} is fixed with no error during modeling with the WD code despite measurement uncertainty which can approach 10% relative standard deviation (R.S.D.) without supporting high resolution spectral data. The effect that such uncertainty in T_{eff1} would have on modeling estimates for q, i, $\Omega_{1,2}$, and T_{eff2} has been investigated with other OCBs, including A- (Alton 2019; Alton *et al.* 2020) and W-subtypes (Alton and Nelson 2018). As might be expected any change in the fixed value for T_{eff1} results in a corresponding change in the T_{eff2}. These findings are consistent whereby the uncertainty in the model fit for T_{eff2} would be essentially the same as that established for T_{eff1}. Furthermore, varying T_{eff1} by as much as 10% did not appreciably affect the uncertainty estimates (R.S.D. <2.2%) for i, q, or $\omega_{1,2}$ (Alton 2019; Alton and Nelson 2018; Alton *et al.* 2020). Assuming that the actual T_{eff1} value falls within 10% of the adopted values used for Roche modeling (a reasonable expectation based on T_{eff1} data provided in Table 5), then uncertainty estimates for i, q, or $\Omega_{1,2}$, along with spot size, temperature, and location, would likely not exceed 2.2% R.S.D.

The fill-out parameter (f) which corresponds to the outer surface shared by each star was calculated according to Equation 8 (Kallrath and Milone 2009; Bradstreet 2005) where:

$$f = (\Omega_{inner} - \Omega_{1,2}) / (\Omega_{inner} - \Omega_{outer}), \qquad (8)$$

wherein Ω_{outer} is the outer critical Roche equipotential, Ω_{inner} is the value for the inner critical Roche equipotential, and $\Omega = \Omega_{1,2}$ denotes the common envelope surface potential for the binary system. In all cases the systems are considered overcontact since $0 < f < 1$.

LC parameters, geometric elements, and their corresponding uncertainties are summarized in Table 6. According to Binnendijk (1970) the deepest minimum (Min I) of a W-type overcontact system occurs when a cooler more massive constituent occludes its hotter but less massive binary partner. The flattened-bottom dip in brightness at Min I (Figure 3) indicates a total eclipse of the secondary star; therefore, WD modeling proceeded under the assumption that V1073 Her is a W-subtype. Since according to the convention used herein whereby the primary star is the most massive ($m_2/m_1 \leq 1$), a phase shift (0.5) was introduced to properly align the LC for subsequent Roche modeling. Except for spot parameters and the fill-out factors, this investigation and that conducted by Samec *et al.* (2014) provided modeling results for V1073 Her that compare quite favorably ($\pm 5\%$).

Spatial renderings (Figure 4) were produced with Binary Maker 3 (BM3; Bradstreet and Steelman 2004) using the final WDWint56a modeling results from 2020. The smaller secondary can be envisioned to completely transit across the primary face during Min II ($\Phi = 0.5$), thereby confirming that the secondary star is totally eclipsed at Min I.

3.5. Preliminary stellar parameters

Mean physical characteristics were estimated for V1073 Her (Table 7) using results from the best fit (spotted) LC simulations from 2020. It is important to note that without the benefit of RV data which define the orbital motion, mass ratio, and total mass of the binary pair, these results should be considered "relative" rather than "absolute" parameters and regarded as preliminary.

Calculations are described below for estimating the solar mass and size, semi-major axis, solar luminosity, bolometric V-mag, and surface gravity of each component. Three empirically derived mass-period relationships (M-PR) for WUMa binaries were used to estimate the primary star mass. The first M-PR was reported by Qian (2003), while two others followed, from Gazeas and Stępień (2008) and then Gazeas (2009). According to Qian (2003), when the primary star is less than $1.35\,M_\odot$ or the system is W-type its mass can be determined from:

$$\log(M_1) = 0.391\,(59) \cdot \log(P) + 1.96\,(17), \qquad (9)$$

where P is the orbital period in days and leads to $M_1 = 0.968 \pm 0.077\,M_\odot$ for the primary. The M-PR derived by Gazeas and Stępień (2008):

$$\log(M_1) = 0.755\,(59) \cdot \log(P) + 0.416\,(24), \qquad (10)$$

corresponds to an OCB system where $M_1 = 1.035 \pm 0.094\,M_\odot$. Gazeas (2009) reported another empirical relationship for the more massive (M_1) star of a contact binary such that:

$$\log(M_1) = 0.725\,(59) \cdot \log(P) - 0.076\,(32) \cdot \log(q) + 0.365\,(32). \quad (11)$$

from which $M_1 = 1.026 \pm 0.069\,M_\odot$. The median of three values ($M_1 = 1.026 \pm 0.010\,M_\odot$) estimated from Equations 9–11 is higher than what might be expected ($0.85\,M_\odot$) for a K1-K2V star. Notwithstanding, the median value was used for subsequent determinations of M_2, semi-major axis a, volume-radii r_L, and bolometric magnitudes (M_{bol}) using the formal errors calculated by WDWint56a (Nelson 2009). The secondary mass = $0.396 \pm 0.006\,M_\odot$ and total mass ($1.422 \pm 0.018\,M_\odot$) were determined using the mean photometric mass ratio ($q_{ptm} = 0.386 \pm 0.001$) derived from the best fit (spotted) models.

The semi-major axis, $a\,(R_\odot) = 2.094 \pm 0.009$, was calculated from Newton's version of Kepler's third law where:

$$a^3 = (G \cdot P^2\,(M_1 + M_2)) / (4\pi^2). \qquad (12)$$

The effective radius of each Roche lobe (r_L) can be calculated over the entire range of mass ratios ($0 < q < \infty$) according to an expression derived by Eggleton (1983):

$$r_L = (0.49q^{2/3}) / (0.6q^{2/3} + \ln(1 + q^{1/3})), \qquad (13)$$

from which values for r_1 (0.4631 ± 0.0003) and r_2 (0.3003 ± 0.0002) were determined for the primary and secondary stars, respectively. Since the semi-major axis and the volume radii are known, the radii in solar units for both binary components can be calculated where $R_1 = a \cdot r_1 = 0.970 \pm 0.004\,R_\odot$ and $R_2 = a \cdot r_2 = 0.629 \pm 0.003\,R_\odot$.

Luminosity in solar units ($L_\odot$) for the primary (L_1) and secondary stars (L_2) was calculated from the well-known

relationship derived from the Stefan-Boltzmann law (Equation 14) where:

$$L_{1,2} = (R_{1,2}/R_\odot)^2 \, (T_{1,2}/T_\odot)^4. \tag{14}$$

Assuming that $T_{eff1} = 5166$ K, $T_{eff2} = 5296$ K, and $T_\odot = 5772$ K, then the solar luminosities ($L_\odot$) for the primary and secondary are $L_1 = 0.603 \pm 0.094$ and $L_2 = 0.280 \pm 0.002$, respectively.

4. Conclusions

Six new times of minimum for V1073 Her based on multicolor CCD data were determined from LCs acquired at two different locations in 2020 and 2021. These, along with other values (n=68) extrapolated from the SuperWASP survey (Butters *et al.* 2010), led to an updated linear ephemeris. At this time it is not possible to firmly establish whether the gravitational effect of a third body or variations in the quadrupole moment is responsible for cyclic changes in the eclipse timing residuals from V1073 Her. The adopted effective temperature ($T_{eff1} = 5166 \pm 201$ K) was based on a composite of sources that included values from photometric and astrometric surveys, and the Gaia DR2 release of stellar characteristics (Andrae *et al.* 2018). V1073 Her experiences a total eclipse from our vantage point which is evident as a flattened bottom during Min I, a characteristic of W-subtype variables. The photometric mass ratio ($q_{ptm} = 0.386 \pm 0.001$) determined by Roche modeling is expected to be a reliable substitute for a mass ratio derived from RV data. Nonetheless, spectroscopic studies (RV and high resolution classification spectra) will be required to unequivocally determine a total mass and spectral class for each system. Consequently, all parameter values and corresponding uncertainties reported herein should be considered preliminary.

5. Acknowledgements

References

Akerlof, C., *et al.* 2000, *Astron. J.*, **119**, 1901.

Alton, K. B. 2019, *J. Amer. Assoc. Var. Star Obs.*, **47**, 7.

Alton, K. B., and Nelson, R. H. 2018, *Mon. Not. Roy. Astron. Soc.*, **479**, 3197.

Alton, K. B., Nelson, R. H., and Stępień, K. 2020, *J. Astrophys. Astron.*, **41**, 26.

Amôres, E. B., and Lépine, J. R. D. 2005, *Astron. J.*, **130**, 659.

Andrae, R., *et al.* 2018, *Astron. Astrophys.*, **616A**, 8.

Applegate, J. H. 1992, *Astrophys. J.*, **385**, 621.

Bailer-Jones, C. A. L. 2015, *Publ. Astron. Soc. Pacific*, **127**, 994.

Berdyugina, S. V. 2005, *Living Rev. Sol. Phys.*, **2**, 8.

Berry, R., and Burnell, J. 2005, *The Handbook of Astronomical Image Processing*, 2nd ed., Willmann-Bell, Richmond, VA.

Binnendijk, L. 1970, *Vistas Astron.*, **12**, 217.

Blättler, E., and Diethelm, R. 2000, *Inf. Bull. Var. Stars*, No. 4975, 1.

Blättler, E., *et al.* 2000, *BBSAG Bull.*, No. 123, 1.

Blättler, E., *et al.* 2001, *BBSAG Bull.*, No. 126, 1.

Blättler, E., *et al.* 2002, *BBSAG Bull.*, No. 128, 1.

Bradstreet, D. H. 2005, in *The Society for Astronomical Sciences 24th Annual Symposium on Telescope Science*, Society for Astronomical Sciences, Rancho Cucamonga, CA, 23.

Bradstreet, D. H., and Steelman, D. P. 2004, BINARY MAKER 3, Contact Software (http://www.binarymaker.com).

Brát, L., Zejda, M., and Svoboda, P. 2007, *Open Eur. J. Var. Stars*, **74**, 1.

Brát, L., *et al.* 2008, *Open Eur. J. Var. Stars*, **94**, 1.

Brát, L., *et al.* 2011, *Open Eur. J. Var. Stars*, **137**, 1.

Butters, O. W., *et al.* 2010, *Astron. Astrophys.*, **520**, L10.

Diethelm, R. 2003, *Inf. Bull. Var. Stars*, No. 5438, 1.

Diethelm, R. 2004, *Inf. Bull. Var. Stars*, No. 5543, 1.

Diethelm, R. 2006, *Inf. Bull. Var. Stars*, No. 5713, 1.

Diethelm, R. 2007, *Inf. Bull. Var. Stars*, No. 5781, 1.

Diethelm, R. 2010, *Inf. Bull. Var. Stars*, No. 5920, 1.

Diethelm, R. 2012, *Inf. Bull. Var. Stars*, No. 6029, 1.

Drake, A. J., *et al.* 2014, *Astrophys. J.*, Suppl. Ser., **213**, 9.

Eggleton, P. P. 1983, *Astrophys. J.*, **268**, 368.

Gaia Collaboration, *et al.* 2016, *Astron. Astrophys.*, **595**A, 1.

Gaia Collaboration, *et al.* 2018, *Astron. Astrophys.*, **616A**, 1.

Gazeas, K. D. 2009, *Commun. Asteroseismology*, **159**, 129.

Gazeas, K., and Stępień, K. 2008, *Mon. Not. Roy. Astron. Soc.*, **390**, 1577.

Gettel, S. J., Geske, M. T., and McKay, T. A. 2006, *Astron. J.*, **131**, 621.

Henden, A. A., Levine, S. E., Terrell, D., Smith, T. C., and Welch, D. L. 2011, *Bull. Amer. Astron. Soc.*, **43**, 2011.

Henden, A. A., Terrell, D., Welch, D., and Smith, T. C. 2010, *Bull. Amer. Astron. Soc.*, **42**, 515.

Henden, A. A., Welch, D. L., Terrell, D., and Levine, S. E. 2009, *Bull. Amer. Astron. Soc.*, **41**, 669.

Hoňková, K., *et al.* 2013, *Open Eur. J. Var. Stars*, **160**, 1.

Hoňková, K., *et al.* 2014, *Open Eur. J. Var. Stars*, **165**, 1.

Houdashelt, M. L., Bell, R. A., and Sweigart, A. V. 2000, *Astron. J.*, **119**, 1448.

Howell, S. B. 2006, *Handbook of CCD Astronomy*, 2nd ed., Cambridge Univ. Press, Cambridge, UK.

Hübscher, J. 2007, *Inf. Bull. Var. Stars*, No. 5802, 1.

Hübscher, J. 2014, *Inf. Bull. Var. Stars*, No. 6118, 1.

Hübscher, J. 2016, *Inf. Bull. Var. Stars*, No. 6157, 1.

Hübscher, J. 2017, *Inf. Bull. Var. Stars*, No. 6196, 1.

Hübscher, J., and Lehmann, P. B. 2012, *Inf. Bull. Var. Stars*, No. 6026, 1.

Hübscher, J., and Lehmann, P. B. 2013, *Inf. Bull. Var. Stars*, No. 6070, 1.

Hübscher, J., and Lehmann, P. B. 2015, *Inf. Bull. Var. Stars*, No. 6149, 1.

Hübscher, J., Lehmann, P. B., and Walter, F. 2012, *Inf. Bull. Var. Stars*, No. 6010, 1.

Hübscher, J., and Monninger, G. 2011, *Inf. Bull. Var. Stars*, No. 5959, 1.

Hübscher, J., Steinbach, H.-M., and Walter, F. 2008, *Inf. Bull. Var. Stars*, No. 5830, 1.

Hübscher, J., Steinbach, H.-M., and Walter, F. 2009, *Inf. Bull. Var. Stars*, No. 5874, 1.

Irwin, J. B. 1959, *Astron. J.*, **64**, 149.

Jayasinghe, T., *et al.* 2018, *Mon. Not. Roy. Astron. Soc.*, **477**, 3145.

Juryšek, J., *et al.* 2017, *Open Eur. J. Var. Stars*, **179**, 1.

Kallrath, J., and Milone, E. F. 2009, *Eclipsing Binary Stars: Modeling and Analysis*, Springer-Verlag, New York.

Kurucz, R. L. 2002, *Baltic Astron.*, **11**, 101.

Kwee, K. K., and van Woerden, H. 1956, *Bull. Astron. Inst. Netherlands*, **12**, 327.

Lucy, L. B. 1967, *Z. Astrophys.*, **65**, 89.

Minor Planet Observer. 2010, MPO Software Suite (http://www.minorplanetobserver.com), BDW Publishing, Colorado Springs.

Mortara, L., and Fowler, A. 1981, in *Solid State Imagers for Astronomy*, SPIE Conf. Proc. 290, Society for Photo-Optical Instrumentation Engineers, Bellingham, WA, 28.

Nagai, K. 2010, *Bull. Var. Star Obs. League Japan*, No. 50, 1.

Nagai, K. 2011, *Bull. Var. Star Obs. League Japan*, No. 51, 1.

Nagai, K. 2012, *Bull. Var. Star Obs. League Japan*, No. 53, 1.

Nagai, K. 2016, *Bull. Var. Star Obs. League Japan*, No. 61, 1.

Nagai, K. 2017, *Bull. Var. Star Obs. League Japan*, No. 63, 1.

Nelson, R. H. 2008, *Inf. Bull. Var. Stars*, No. 5820, 1.

Nelson, R. H. 2009, *Inf. Bull. Var. Stars*, No. 5875, 1.

Nelson, R. H. 2009, WDwint56a: Astronomy Software by Bob Nelson (https://www.variablestarssouth.org/bob-nelson).

Nelson, R. H. 2013, *Inf. Bull. Var. Stars*, No. 6050, 1.

Pagel, L. 2018a, *Inf. Bull. Var. Stars*, No. 6244, 1.

Pagel, L. 2018b, *BAV Journal*, No. 31, 1.

Pagel, L. 2021, *BAV Journal*, No. 52, 1.

Paunzen, E., and Vanmunster, T. 2016, *Astron. Nachr.*, **337**, 239.

Pecaut, M., and Mamajek, E. E. 2013, *Astrophys. J., Suppl. Ser.*, **208**, 9.

Pribulla, T., and Ruciński, S. M. 2006, *Astron. J.*, **131**, 2986.

Prša, A., and Zwitter, T. 2005, *Astrophys. J.*, **628**, 426.

Qian, S. 2003, *Mon. Not. Roy. Astron. Soc.*, **342**, 1260.

Ruciński, S. M. 1969, *Acta Astron.*, **19**, 245.

Samec, R. G., Kring, J., Benkendorf, J., Dignan, J., van Hamme, W., and Faulkner, D. R. 2014, *J. Amer. Assoc. Var. Star Obs.*, **42**, 406.

Shappee, B. J., *et al.* 2014, *Astrophys. J.*, **788**, 48.

Smith, T. C., Henden, A. A., and Starkey, D. R. 2011, in *The Society for Astronomical Sciences 30th Annual Symposium on Telescope Science*, Society for Astronomical Sciences, Rancho Cucamonga, CA, 121.

Software Bisque. 2019, TheSkyX professional edition 10.5.0 (https://www.bisque.com).

Terrell, D., and Wilson, R. E. 2005, *Astrophys. Space Sci.*, **296**, 221.

Tian, Y. P., Xiang, F. Y., and Tao, X. 2009, *Astrophys. Space Sci.*, **319**, 119.

van Hamme, W. 1993, *Astron. J.*, **106**, 2096.

Völschow, M., Schleicher, D. R. G., Perdelwitz, V., and Banerjee, R. 2016, *Astron. Astrophys.*, **587A**, 34.

Watson, C., Henden, A. A., and Price, C. A. 2014, AAVSO International Variable Star Index VSX (Watson+, 2006–2014; https://www.aavso.org/vsx).

Wilson, R. E. 1979, *Astrophys. J.*, **234**, 1054.

Wilson, R. E. 1990, *Astrophys. J.*, **356**, 613.

Wilson, R. E., and Devinney, E. J., 1971, *Astrophys. J.*, **166**, 605.

Woźniak, P. R., *et al.* 2004, *Astron. J.*, **127**, 2436.

Zasche, P., Liakos, A., Niarchos, P., Wolf, M., Manimanis, V., and Gazeas, K. 2009, *New Astron.*, **14**, 121.